

# Non-intrusive model reduction of large-scale, nonlinear dynamical systems using deep learning

Han Gao<sup>a,b</sup>, Jian-Xun Wang<sup>a,b</sup>, Matthew J. Zahr<sup>a,b,\*</sup>

<sup>a</sup>*Department of Aerospace and Mechanical Engineering, University of Notre Dame, Notre Dame, IN*

<sup>b</sup>*Center for Informatics and Computational Science, University of Notre Dame, Notre Dame, IN*

---

## Abstract

Projection-based model reduction has become a popular approach to reduce the cost associated with integrating large-scale dynamical systems so they can be used in many-query settings such as optimization and uncertainty quantification. For nonlinear systems, significant cost reduction is only possible with an additional layer of approximation to reduce the computational bottleneck of evaluating the projected nonlinear terms. Prevailing methods to approximate the nonlinear terms are code intrusive, potentially requiring years of development time to integrate into an existing codebase, and have been known to lack parametric robustness.

This work develops a non-intrusive method to efficiently and accurately approximate the expensive nonlinear terms that arise in reduced nonlinear dynamical system using deep neural networks. The neural network is trained using only the simulation data used to construct the reduced basis and evaluations of the nonlinear terms at these snapshots. Once trained, the neural network-based reduced-order model only requires forward and backward propagation through the network to evaluate the nonlinear term and its derivative, which are used to integrate the reduced dynamical system at a new parameter configuration. We provide two numerical experiments—the dynamical systems result from the semi-discretization of parametrized, nonlinear, hyperbolic partial differential equations—that show, in addition to non-intrusivity, the proposed approach provides more stable and accurate approximations to each dynamical system across a large number of training and testing points than the popular empirical interpolation method.

*Keywords:* nonlinear model reduction, non-intrusive hyperreduction, deep learning

---

## 1. Introduction

Numerical simulations have made an undeniable impact on the fields of science, engineering, and medicine due to the possibility to study or analyze a physical system in a virtual setting. However, modeling and simulation of most practical systems is a computationally expensive endeavor, usually requiring days on a supercomputer, essentially limiting users to a few runs. However, the true power of computational physics lies in many-query analyses, e.g., optimization and uncertainty quantification (UQ), which require simulations at a large number of parameter configurations. For example, optimization problems are ubiquitous in science and engineering and their solutions can lead to systems with unprecedented efficiency (e.g., energetically optimal flapping flight [1–4]), help gain insight to physical phenomena, or determine properties of a system from sparse, noisy observations of the solution (inverse problems). To enable these types of many-query analyses on important problems, the issue of high computational cost of a single simulation must be addressed. Reduced-order models (ROMs) offer a promising means to do so.

The number of degrees of freedom (DOF) of a dynamical system is dramatically reduced in ROMs by constraining the dynamics to evolve in a very low-dimensional subspace, spanned by a set of reduced basis (RB) functions. These basis functions are usually learned through training data, i.e., solution snapshots obtained from high-dimensional model (HDM) simulations. Although the number of DOF can be significantly

---

\*Corresponding author. Tel: +1 574-631-1298

Email address: mzahr@nd.edu (Matthew J. Zahr)

reduced by RB projection, for nonlinear problems, the speedup of the standard ROMs is often marginal due to a large number of high-dimensional operations involved in the evaluation of nonlinear terms in the ROM system. Therefore, an additional step, usually called *hyperreduction*, must be taken to efficiently approximate nonlinear terms. Most existing hyperreduction techniques, e.g., empirical interpolation method (EIM) [5] and its discrete variant discrete EIM (DEIM) [6], approximate the HDM nonlinear velocity function using a low-dimensional subspace as well, which provides a satisfactory tool to deal with nonlinear PDE systems in an efficient way. Massive speedups can be gained by hyperreduced ROMs in many cases where the solution of a dynamical system and its nonlinear terms are well-approximated in low-dimensional subspaces, including non-parametric problems (reproduce training data), linear elliptic PDEs, or problems with limited parameter variations [7–9].

Despite the tremendous promise of ROMs, standard hyperreduction techniques often struggle to provide a stable and accurate approximation of nonlinear terms and present notable limitations in parametric settings [10]. This lack of parametric robustness remains the main roadblock of ROMs being the technology that enables large-scale many-query analyses which inherently involve parametric variations. In addition, standard hyperreduction techniques are code intrusive [6], usually requiring hundreds of person-hours to implement, which poses great challenges to leveraging existing open-source or commercial legacy codes for computational mechanics. Therefore, there is an increasing interest in developing non-intrusive or weakly-intrusive ROMs without the need for access to HDM operators to achieve better robustness and stability [11–14]. For example, Audouze et al. [11] proposed a non-intrusive proper orthogonal decomposition (POD)-based ROM, where the Galerkin projection is bypassed by using a radial basis regression to estimate the RB coefficients directly and does not require hyperreduction for efficiency. Peherstofer and Wilcox [12] proposed a data-driven operator inference approach based on least square fitting to establish a non-intrusive projection-based ROM framework. Reduced-order models based on piecewise polynomial approximation of the dynamical system in state space [15, 16] are popular in subsurface flow [17–19] and electrical engineering applications [15, 20], but are difficult to train since they sensitive to the choice of expansion points [21].

Recent advances in scientific machine learning (SciML) has been receiving increased attention in the computational modeling community [22–26] and offers new opportunities to develop more efficient and accurate reduced-order models. A growing amount of research using machine learning, particularly deep learning techniques, for model reduction has been witnessed most recently. Specifically, a majority of these studies focused on learning the closure model (or discrepancy terms) of projection-based ROMs from data to improve their predictive accuracy [27–34]. San and Maulik [28, 29] employed feedforward neural networks (NNs) to build the ROM closures, with which the performance can be notably improved. Pan and Duraisamy [30] modeled the truncated dynamics in a data-driven way using sparse regression and neural networks. In a similar vein, Mohebujjaman et al. [32] proposed a data-driven correction ROM (DDC-ROM) framework, which has been tested on a number of fluid dynamic problems. In addition to building closure models, machine learning has also been used to construct more representative basis functions for model reduction. For example, Lee and Carlberg [22] applied deep convolutional autoencoders to learn the nonlinear manifold defined by the parametrized dynamical system solution, which was shown to outperform the linear POD basis. Another important direction of using machine learning in model reduction is the development of accurate non-intrusive ROMs [35–49]. In most of these works, the general idea is to use machine learning models to learn the temporal evolution of the states in the reduced subspace and thus the Galerkin projection and intrusive hyperreduction are bypassed. For example, the dynamics in low-dimensional manifold can be learned using a multi-level perceptrons (MLP) [39, 40, 42], deep residual recurrent neural networks (RNN) [36], or Long Short Term Memory (LSTM) based RNN [37, 43, 49]. Most of these approaches are purely data-driven and equation-free, which makes it difficult to respect the underlying PDE structure. Moreover, these works are focused on problems with non-parametric settings [44, 49].

In this work, we propose a novel method to approximate the nonlinear terms arising in projection-based ROMs that uses deep learning (DL) to overcome the parametric robustness issues and code intrusion of existing hyperreduction methods. Namely, a deep fully-connected neural network (NN) will be built to learn the nonlinear velocity function in the ROM equations by leveraging the same HDM solution data used to construct the POD basis and the corresponding velocity data. The deep NN model here is embedded into the standard projection-based ROM setting and the resulting dynamical system is solved using numerical time integration. The proposed method is *non-intrusive* in the sense that the hyperreduced model is a small dynamical system with velocity function defined by the NN that can be run independently of the original

simulation code once the NN has been trained. The performance of the proposed method will be compared against a ROM without hyperreduction and a ROM with the (D)EIM hyperreduction. Note that this work is focused on parametrized, nonlinear dynamical systems. To the best of our knowledge, the current work is the first attempt to build a DL-based hyperreduction for projection-based ROMs in parametric settings.

The rest of the paper is organized as follows. Section 2 introduces projection-based model reduction for nonlinear dynamical systems and briefly discusses the popular, intrusive hyperreduction method (D)EIM. Section 3 presents the detailed formulation and training procedure for the proposed non-intrusive reduced-order model that uses deep learning to approximate the reduced velocity function. Section 4 compares the accuracy of the proposed method against classical model reduction and (D)EIM using two dynamical systems that result from the semi-discretization of nonlinear, hyperbolic PDEs. Finally, Section 5 concludes the paper.

## 2. Classical model reduction of nonlinear dynamical systems

### 2.1. Large-scale, nonlinear dynamical system

Consider a parametrized, nonlinear dynamical system that we will take to be the HDM,

$$\mathbf{M} \frac{d\mathbf{u}}{dt} = \mathbf{f}(\mathbf{u}, t, \boldsymbol{\mu}), \quad \mathbf{u}(0) = \mathbf{u}_0, \quad (1)$$

where  $\mathcal{D} \subset \mathbb{R}^{N_\mu}$  is the parameter space,  $\mathbf{u} : [0, T] \times \mathcal{D} \rightarrow \mathbb{R}^{N_u}$  is the time- and parameter-dependent state,  $\mathbf{u}_0 \in \mathbb{R}^{N_u}$  is the initial condition,  $\mathbf{f} : \mathbb{R}^{N_u} \times [0, T] \times \mathcal{D} \rightarrow \mathbb{R}^{N_u}$  is the velocity of the nonlinear dynamical system  $(\boldsymbol{\xi}, t, \boldsymbol{\mu}) \mapsto \mathbf{f}(\boldsymbol{\xi}, t, \boldsymbol{\mu})$ , and  $\mathbf{M} \in \mathbb{R}^{N_u \times N_u}$  is the mass matrix. To approximately integrate the system in (1), we introduce a discretization of the time domain into  $N_t$  intervals with endpoints  $\mathcal{T} := \{t_0, t_1, \dots, t_{N_t}\}$  such that  $t_0 = 0$ ,  $t_{N_t} = T$ , and  $t_n < t_{n+1}$  for  $n = 0, \dots, N_t - 1$  and use any standard solver, e.g., backward differentiation formulas or Runge-Kutta methods, to approximate the solution at these nodes. In this work, we assume the system in (1) is large-scale ( $N_u \gg 1$ ) and computationally intensive to numerically integrate. Of particular interest are dynamical systems that result from the semi-discretization of partial differential equations for large, complex systems, e.g., in computational fluid dynamics it is not uncommon to have semi-discrete models with  $\mathcal{O}(10^8)$  degrees of freedom [7, 10].

We assume the computational complexity of evaluating the  $N_u$ -components of the velocity function  $(\boldsymbol{\xi}, t, \boldsymbol{\mu}) \mapsto \mathbf{f}(\boldsymbol{\xi}, t, \boldsymbol{\mu})$  is  $\mathcal{O}(g(N_u))$ . Furthermore, we assume the complexity of evaluating the Jacobian matrix  $(\boldsymbol{\xi}, t, \boldsymbol{\mu}) \mapsto \frac{\partial \mathbf{f}}{\partial \boldsymbol{\xi}}(\boldsymbol{\xi}, t, \boldsymbol{\mu})$  is also  $\mathcal{O}(g(N_u))$ . This holds for local discretizations such as the finite difference, finite element, or finite volume methods where the Jacobian is sparse with the number of nonzeros per column and computational complexity of evaluating each column independent of  $N_u$ . The complexity of an entire implicit time step—dominated by the velocity and Jacobian evaluation and the linear solve with the Jacobian matrix—is  $\mathcal{O}(g(N_u) + N_u^3)$  if a direct solver is used and  $\mathcal{O}(g(N_u) + N_u^2)$  if an iterative solver with an effective preconditioner is used.

### 2.2. Projection-based model order reduction

The construction of projection-based reduced-order models begins with the ansatz that the solution of the dynamical system can be well-approximated in a low-dimensional affine subspace  $\mathcal{V} := \{\bar{\mathbf{u}} + \boldsymbol{\Phi} \mathbf{y} \mid \mathbf{y} \in \mathbb{R}^{k_u}\}$ , where  $\boldsymbol{\Phi} \in \mathbb{R}^{N_u \times k_u}$  with  $\boldsymbol{\Phi}^T \boldsymbol{\Phi} = \mathbf{I}$  denotes the reduced basis of dimension  $k_u \ll N_u$  and  $\bar{\mathbf{u}} \in \mathbb{R}^{N_u}$  is an affine offset. That is,

$$\mathbf{u}(t, \boldsymbol{\mu}) \approx \mathbf{u}_r(t, \boldsymbol{\mu}) := \bar{\mathbf{u}} + \boldsymbol{\Phi} \mathbf{y}(t, \boldsymbol{\mu}), \quad (2)$$

where  $\mathbf{u}_r : [0, T] \times \mathcal{D} \rightarrow \mathcal{V}$  is the approximation of  $\mathbf{u}(t, \boldsymbol{\mu})$  in the reduced subspace and  $\mathbf{y} : [0, T] \times \mathcal{D} \rightarrow \mathbb{R}^{k_u}$  are the reduced coordinates of  $\mathbf{u}_r(t, \boldsymbol{\mu})$  corresponding to the basis  $\boldsymbol{\Phi}$  and offset  $\bar{\mathbf{u}}$ . The reduced coordinates are defined by enforcing the subspace approximation (2) in the governing equation and constraining the resulting system to be orthogonal to a test subspace  $\mathcal{W}$  of dimension  $\dim \mathcal{W} = k_u$

$$\mathbf{M}_r \frac{d\mathbf{y}}{dt} = \mathbf{f}_r(\mathbf{y}, t, \boldsymbol{\mu}), \quad \mathbf{y}(0) = \mathbf{y}_0, \quad (3)$$

where  $\boldsymbol{\Psi} \in \mathbb{R}^{N_u \times k_u}$  with  $\boldsymbol{\Psi}^T \boldsymbol{\Psi} = \mathbf{I}$  is a basis for  $\mathcal{W}$ . The velocity of the reduced dynamical system is

$$\mathbf{f}_r : \mathbb{R}^{k_u} \times [0, T] \times \mathcal{D} \rightarrow \mathbb{R}^{k_u}, \quad (\boldsymbol{\tau}, t, \boldsymbol{\mu}) \mapsto \boldsymbol{\Psi}^T \mathbf{f}(\bar{\mathbf{u}} + \boldsymbol{\Phi} \boldsymbol{\tau}, t, \boldsymbol{\mu}) \quad (4)$$

and the reduced mass matrix  $\mathbf{M}_r \in \mathbb{R}^{k_u \times k_u}$  and initial condition for the reduced coordinates  $\mathbf{y}_0 \in \mathbb{R}^{k_u}$  are defined as

$$\mathbf{M}_r := \Psi^T \mathbf{M} \Phi, \quad \mathbf{y}_0 := \Phi^T (\mathbf{u}_0 - \bar{\mathbf{u}}). \quad (5)$$

The reduced initial condition  $\mathbf{y}_0$  is the orthogonal projection of the initial condition  $\mathbf{u}_0$  onto the trial subspace.

In this work, we choose the test space to be the same as the trial space, up to the affine offset, i.e., a Galerkin projection  $\Psi = \Phi$ . The affine offset is taken to be the initial condition  $\bar{\mathbf{u}} = \mathbf{u}_0$  based on the observations in [50]. The reduced basis  $\Phi$  is defined using the method of snapshots and proper orthogonal decomposition (POD) [51]. For each parameter in a given training set  $\Xi_0 := \{\boldsymbol{\mu}_1, \dots, \boldsymbol{\mu}_{N_s}\} \subset \mathcal{D}$ , we compute the approximate solution on the time discretization  $\mathcal{T}$  and agglomerate into a global snapshot matrix  $\mathbf{X} = [\mathbf{X}_1 \ \dots \ \mathbf{X}_{N_s}] \in \mathbb{R}^{N_u \times N_t N_s}$ , where fixed-parameter snapshot matrices  $\mathbf{X}_k \in \mathbb{R}^{N_u \times N_t}$  are defined as

$$\mathbf{X}_k := [\mathbf{u}(t_1, \boldsymbol{\mu}_k) \ \dots \ \mathbf{u}(t_{N_t}, \boldsymbol{\mu}_k)] \quad (6)$$

for  $k = 1, \dots, N_s$ . The reduced basis  $\Phi$  is defined by compressing the information in the snapshot matrix using POD, i.e., retaining the dominant singular vectors of the translated snapshot matrix  $\mathbf{u} - \mathbf{u}_0 \mathbf{1}^T$  (to account for the affine offset). This computationally expensive *training phase* requires  $N_s$  solutions of the large-scale dynamical system and compression of the resulting snapshot matrix of size  $N_u \times N_s N_t$ , but is only required once; the resulting reduced-order model can be leveraged on a testing set  $\Xi^*$  without re-training to ameliorate the offline cost. Generalizability of the basis to  $\Xi^*$  depends on the coverage of the parameter space with training samples. Sophisticated greedy methods exist to select training samples based on the maximum ROM error in the parameter space [52, 53], given a reliable error indicator is available. Since we consider complex nonlinear problems, such error indicators with high effectivity are not available so we simply use uniform sampling—feasible in our setting due to low-dimensional parameter spaces considered ( $N_\mu \leq 3$  in Section 4)—to ensure sufficient coverage of the parameter space.

The computational cost of integrating the ROM (3) is dominated by the evaluation of the reduced velocity function and its Jacobian and the linear solve with the Jacobian matrix. The computational complexity of evaluating the reduced velocity function  $(\boldsymbol{\tau}, t, \boldsymbol{\mu}) \mapsto \mathbf{f}_r(\boldsymbol{\tau}, t, \boldsymbol{\mu})$  and its Jacobian  $(\boldsymbol{\tau}, t, \boldsymbol{\mu}) \mapsto \frac{\partial \mathbf{f}_r}{\partial \boldsymbol{\tau}}(\boldsymbol{\tau}, t, \boldsymbol{\mu})$  are  $\mathcal{O}(g(N_u) + N_u k_u)$  and  $\mathcal{O}(g(N_u) + N_u k_u^2)$ , respectively. An entire implicit time step requires  $\mathcal{O}(g(N_u) + N_u k_u^2 + k_u^3)$  operations, assuming a direct solver is used for the linear system of equations, which is almost exclusively the case due to the small size of  $k_u$ .

### 2.3. Hyperreduction to accelerate projection of nonlinear terms

Despite the substantial reduction in the dimensionality of the dynamical system, from  $N_u$ -dimensional in (1) to  $k_u$ -dimensional in (3) with  $k_u \ll N_u$ , it is well-known the ROM only achieves marginal speedup relative to the HDM due to an inherent bottleneck in the evaluation of the nonlinear term  $\mathbf{f}_r(\boldsymbol{\tau}, t, \boldsymbol{\mu})$  with complexity proportional to the large dimension  $N_u$ :  $\mathcal{O}(g(N_u) + N_u k_u)$ . From the definition in (4) it is clear that even though  $\mathbf{f}_r$  is a mapping between low-dimensional spaces, it is expensive to evaluate due to a sequence of high-dimensional operations: reconstruction of  $\mathbf{u}_r = \bar{\mathbf{u}} + \Phi \boldsymbol{\tau}$  ( $\mathcal{O}(N_u k_u)$  operations), evaluation of the HDM velocity function  $\mathbf{f}(\mathbf{u}_r, t, \boldsymbol{\mu})$  ( $\mathcal{O}(g(N_u))$  operations), and projection of the velocity onto  $\text{Range}(\Phi)$  ( $\mathcal{O}(N_u k_u)$  operations). To overcome this computational bottleneck, a host of so-called *hyperreduction* methods [5–9, 54–58] have been introduced to approximate  $\mathbf{f}_r$  at a cost that does not scale with  $N_u$ . However, these methods usually have limited prediction potential for complex problems [10] and, most importantly, are difficult and code-intrusive to implement properly and achieve substantial speedup in practice.

For example, the empirical interpolation method [5] and its discrete variant [6] approximate the ROM velocity function as

$$\mathbf{f}_r(\boldsymbol{\tau}, t, \boldsymbol{\mu}) \approx \mathbf{f}_d(\boldsymbol{\tau}, t, \boldsymbol{\mu}) := \mathbf{A} \mathbf{P}^T \mathbf{f}(\bar{\mathbf{u}} + \Phi \boldsymbol{\tau}, t, \boldsymbol{\mu}), \quad \mathbf{A} = \Psi^T \mathbf{\Pi} (\mathbf{P}^T \mathbf{\Pi})^{-1} \in \mathbb{R}^{k_u \times k_f}, \quad (7)$$

where  $\mathbf{\Pi} \in \mathbb{R}^{N_u \times k_f}$  is a basis for a  $k_f$ -dimensional subspace ( $k_f \ll N_u$ ) used to approximate the HDM velocity function  $\mathbf{f}$  and  $\mathbf{P} \in \mathbb{R}^{N_u \times k_f}$  is a subset of the columns of the  $N_u \times N_u$  identity matrix used to sample entries of the HDM velocity function. Then the (D)EIM reduced coordinates  $\mathbf{y}_d : [0, T] \times \mathcal{D} \rightarrow \mathbb{R}^{k_u}$  are computed such that

$$\mathbf{M}_r \frac{d\mathbf{y}_d}{dt} = \mathbf{f}_d(\mathbf{y}_d, t, \boldsymbol{\mu}), \quad \mathbf{y}_d(0) = \mathbf{y}_0, \quad (8)$$

and the HDM approximation  $\mathbf{u}_d : [0, T] \times \mathcal{D} \rightarrow \mathbb{R}^{N_u}$  is reconstructed as

$$\mathbf{u}(t, \boldsymbol{\mu}) \approx \mathbf{u}_d(t, \boldsymbol{\mu}) := \bar{\mathbf{u}} + \Phi \mathbf{y}_d(t, \boldsymbol{\mu}). \quad (9)$$

As noted in [6, 8, 59], for this approach to be efficient, it is not sufficient to first evaluate  $\mathbf{f}(\bar{\mathbf{u}} + \Phi \boldsymbol{\tau}, t, \boldsymbol{\mu})$  and then sample its entries. Rather, the term  $\mathbf{P}^T \mathbf{f}$  must be evaluated directly given the appropriate sampling of the state  $\hat{\mathbf{P}}^T \mathbf{u}$ , where  $\hat{\mathbf{P}} \in \mathbb{R}^{N_u \times k_s}$  is the matrix that samples all entries of the state  $\mathbf{u}$  required to evaluate the entries necessary entries of the velocity function  $\mathbf{P}^T \mathbf{f}$ . This approach assumes sparse dependence of the velocity function on the state, i.e., each entry of the velocity function depends on a small number of entries of the state vector. This sparsity property is guaranteed if the dynamical system in (1) corresponds to the semi-discretization of a PDE using local methods e.g., finite difference or finite volume methods. Direct implementation of  $\mathbf{P}^T \mathbf{f}$  given  $\hat{\mathbf{P}}^T \mathbf{u}$  in the context of a PDE discretization involves the use of a sparsified or sample mesh on which the state  $\hat{\mathbf{P}}^T \mathbf{u}$  is defined [6]. While successful, this approach is code intrusive and difficult to implement, often requiring years of development to incorporate into existing codes. In addition, the implementation is highly dependent on the semi-discretization approach used for the PDE [6–8, 57, 58]. Other physics-based hyperreduction methods besides (D)EIM exist [5–9, 54–58] to approximate the ROM velocity; however, they all rely on this concept of partial assembly over a sample mesh and require a specialized, code-intrusive implementation.

Assuming an efficient implementation of the sampled nonlinear velocity function and its Jacobian, the computational complexity of evaluating each term is  $\mathcal{O}(g(k_f) + k_f k_u)$  and  $\mathcal{O}(g(k_f) + k_f k_u^2 + \gamma k_f k_u)$  [6], respectively, where  $\gamma$  is the average number of nonzero entries per column of the full Jacobian matrix  $\frac{\partial \mathbf{f}}{\partial \boldsymbol{\xi}}$ . In this work, we assume  $\gamma$  is independent of  $N_u$ , which simplifies the complexity of the reduced Jacobian evaluation to  $\mathcal{O}(g(k_f) + k_f k_u^2)$ . An implicit time step requires  $\mathcal{O}(g(k_f) + k_f k_u^2 + k_u^3)$  operations, assuming a direct solver is used for the linear system of equations, which is independent of  $N_u$  and substantially cheaper than integrating the HDM (1) and ROM without hyperreduction (3).

### 3. Non-intrusive hyperreduction using deep neural networks

We propose a new approach to hyperreduction that approximates the ROM velocity function using a deep neural network, which we abbreviate ROM-NN in the remainder. That is, we introduce a function

$$\hat{\mathbf{f}}_r : \mathbb{R}^{k_u} \times [0, T] \times \mathcal{D} \times \mathbb{R}^{N_w} \rightarrow \mathbb{R}^{k_u}, \quad (\boldsymbol{\tau}, t, \boldsymbol{\mu}, \boldsymbol{\nu}) \mapsto \hat{\mathbf{f}}_r(\boldsymbol{\tau}, t, \boldsymbol{\mu}; \boldsymbol{\nu}) \quad (10)$$

and vector of weights  $\mathbf{w} \in \mathbb{R}^{N_w}$  such that

$$\hat{\mathbf{f}}_r(\mathbf{y}(t, \boldsymbol{\mu}), t, \boldsymbol{\mu}; \mathbf{w}) \approx \mathbf{f}_r(\mathbf{y}(t, \boldsymbol{\mu}), t, \boldsymbol{\mu}) \quad (11)$$

for any  $t \in [0, T]$  and  $\boldsymbol{\mu} \in \mathcal{D}$  and compute  $\mathbf{y}_n : [0, T] \times \mathcal{D} \rightarrow \mathbb{R}^{k_u}$  that solves

$$\mathbf{M}_r \frac{d\mathbf{y}_n}{dt} = \hat{\mathbf{f}}_r(\mathbf{y}_n, t, \boldsymbol{\mu}), \quad \mathbf{y}_n(0) = \mathbf{y}_0. \quad (12)$$

The HDM approximation  $\mathbf{u}_n : [0, T] \times \mathcal{D} \rightarrow \mathbb{R}^{N_u}$  is reconstructed as

$$\mathbf{u}(t, \boldsymbol{\mu}) \approx \mathbf{u}_n(t, \boldsymbol{\mu}) := \bar{\mathbf{u}} + \Phi \mathbf{y}_n(t, \boldsymbol{\mu}). \quad (13)$$

If (11) holds, we expect  $\mathbf{y}_n$  to be a good approximation to  $\mathbf{y}$  and, provided the reduced basis is sufficient,  $\mathbf{u}_n$  to be a good approximation to  $\mathbf{u}$ .

The ROM velocity (4) is a  $k_u$ -valued function of  $k_u + 1 + N_\mu$  variables; training a neural network to approximate this mapping requires a (large) number of instances of the function input  $(\boldsymbol{\tau}, t, \boldsymbol{\mu}) \in \mathbb{R}^{k_u} \times [0, T] \times \mathcal{D}$  and the corresponding output  $\mathbf{f}_r(\boldsymbol{\tau}, t, \boldsymbol{\mu}) \in \mathbb{R}^{k_u}$  so the network weights can be tuned to minimize a loss function. In this work, the network weights are defined as the solution of the following optimization problem

$$\underset{\mathbf{w} \in \mathbb{R}^{N_w}}{\text{minimize}} \quad \frac{1}{2} \sum_{i=1}^{N_t} \sum_{j=1}^{N_s} \left\| \hat{\mathbf{f}}_r(\boldsymbol{\tau}_{ij}, t_i, \boldsymbol{\mu}_j; \mathbf{w}) - \mathbf{f}_r(\boldsymbol{\tau}_{ij}, t_i, \boldsymbol{\mu}_j) \right\|_2^2, \quad (14)$$

where  $\{t_i\}_{i=1}^{N_t} \subset [0, T]$  are the nodes of the temporal discretization (Section 2.1),  $\{\boldsymbol{\mu}_k\}_{k=1}^{N_s} \subset \mathcal{D}$  are the training parameters (Section 2.2), and  $\boldsymbol{\tau}_{ij} \in \mathbb{R}^{k_u}$  for  $i = 1, \dots, N_t, j = 1, \dots, N_s$  are the reduced coordinates used for training the network. Given the requirement in (11) that the DNN velocity function matches the ROM velocity function *on the manifold of ROM solutions*, a sensible choice is  $\boldsymbol{\tau}_{ij} = \mathbf{y}(t_i, \boldsymbol{\mu}_j)$ . While consistent with the requirement in (11), this approach requires that both the HDM solution  $\mathbf{u}(t, \boldsymbol{\mu})$  and expensive ROM solution  $\mathbf{y}(t, \boldsymbol{\mu})$ , i.e., without hyperreduction, be computed for each  $\boldsymbol{\mu} \in \Xi_0$  to define the training data, which can substantially increase the offline cost. To mitigate the additional cost of computing the expensive ROM solution, we propose to use the projection of the HDM solution onto the subspace  $\mathcal{V}$  in place of the ROM solution itself. That is, we take  $\boldsymbol{\tau}_{ij} = \tilde{\mathbf{y}}(t_i, \boldsymbol{\mu}_j)$ , where

$$\tilde{\mathbf{y}} : [0, T] \times \mathcal{D} \rightarrow \mathbb{R}^{k_u}, \quad (t, \boldsymbol{\mu}) \mapsto \Phi^T(\mathbf{u}(t, \boldsymbol{\mu}) - \bar{\mathbf{u}}), \quad (15)$$

which requires exactly the *same* data used to compute the reduced basis  $\Phi$ . The complete training procedure is summarized in Algorithm 1.

---

**Algorithm 1** Training procedure for deep learning-based reduced-order model

---

**Input:** Training set  $\{\boldsymbol{\mu}_j\}_{j=1}^{N_s} \subset \mathcal{D}$ , temporal discretization  $\{t_i\}_{i=1}^{N_t} \subset [0, T]$ , initial condition  $\mathbf{u}_0 \in \mathbb{R}^{N_u}$

**Output:** Affine offset  $\bar{\mathbf{u}} \in \mathbb{R}^{N_u}$ , reduced basis  $\Phi \in \mathbb{R}^{N_u \times k_u}$ , network weights  $\mathbf{w} \in \mathbb{R}^{N_w}$

- 1: **for**  $j = 1, \dots, N_s$  **do**
  - 2:   Compute solution of the HDM dynamical system  $\mathbf{u}(\cdot, \boldsymbol{\mu}_j)$
  - 3: **end for**
  - 4: Define the snapshot matrix  $\mathbf{X} \in \mathbb{R}^{N_u \times N_s N_t}$  according to (6)
  - 5: Compute the left singular vectors of  $\mathbf{X} - u_0 \mathbf{1}^T$ :  $\mathbf{u}_i \in \mathbb{R}^{N_u}$ ,  $i = 1, \dots, N_s N_t$
  - 6: Define reduced subspace:  $\bar{\mathbf{u}} \leftarrow \mathbf{u}_0$ ,  $\Phi \leftarrow [\mathbf{u}_1 \ \cdots \ \mathbf{u}_r]$
  - 7: **for**  $j = 1, \dots, N_s$  **do**
  - 8:   **for**  $i = 1, \dots, N_t$  **do**
  - 9:     Compute  $\boldsymbol{\tau}_{ij} = \Phi^T(\mathbf{u}(t_i, \boldsymbol{\mu}_j) - \bar{\mathbf{u}})$
  - 10:   **end for**
  - 11: **end for**
  - 12: Solve (14) for network weights  $\mathbf{w}$
- 

In this work, we define  $\hat{\mathbf{f}}_r$  using a fully-connected, feed-forward neural network (FCNN) architecture, which contains one input layer (the input vector  $(\boldsymbol{\tau}, t, \boldsymbol{\mu})$ ), five hidden layers, and one output layer (the prediction  $\hat{\mathbf{f}}_r(\boldsymbol{\tau}, t, \boldsymbol{\mu})$ ). Each layer is fed forward to the next layer by a linear weighted sum and nonlinear activation function (e.g., ReLU). The network is built in the form of sparse autoencoder (SAE), namely the hidden layers follow a decoder-encoder structure in order to capture the complex hidden nonlinear pattern of the mapping. The number of neurons for each layers from the input to the output are (80, 120, 240, 480, 240, 120, 80). Standardized normalization is applied for both input and output layers. The training is conducted in a supervised manner, i.e., minimizing the loss function of data misfit, using a stochastic gradient descent (SGD) based optimizer (e.g. Adam algorithm [60]). To avoid over-fitting, the dropout [61] and early stopping [62] techniques are applied. To demonstrate the robustness of the ROM-NN, the architecture and hyperparameters of the network remain the same for all test cases throughout the paper. We considered a number of other FCNN structures (uniform, converging-diverging, diverging-converging; Figure 1) of varying depths and breadths and found the accuracy of the ROM-NN to be rather insensitive to the network structure; for the problems considered, even a shallow neural network with only two hidden layers and 80 neurons per layer leads to a ROM-NN with similar overall accuracy as one with the aforementioned diverging-converging structure. The only exception being in the limit of sparse training where a deeper network leads to a slightly more accurate ROM-NN.

This approach is guaranteed to be *non-intrusive* because the training procedure only relies on snapshots of the HDM solutions and evaluations of the ROM velocity function and the online solution only requires evaluation of the neural network velocity function (forward pass) and its derivative with respect to  $\boldsymbol{\tau}$  (backward propagation). As a result, both the DNN and dynamical system code can be treated as *black boxes*, which substantially eases the implementation burden. Another advantage of the proposed ROM-NN method

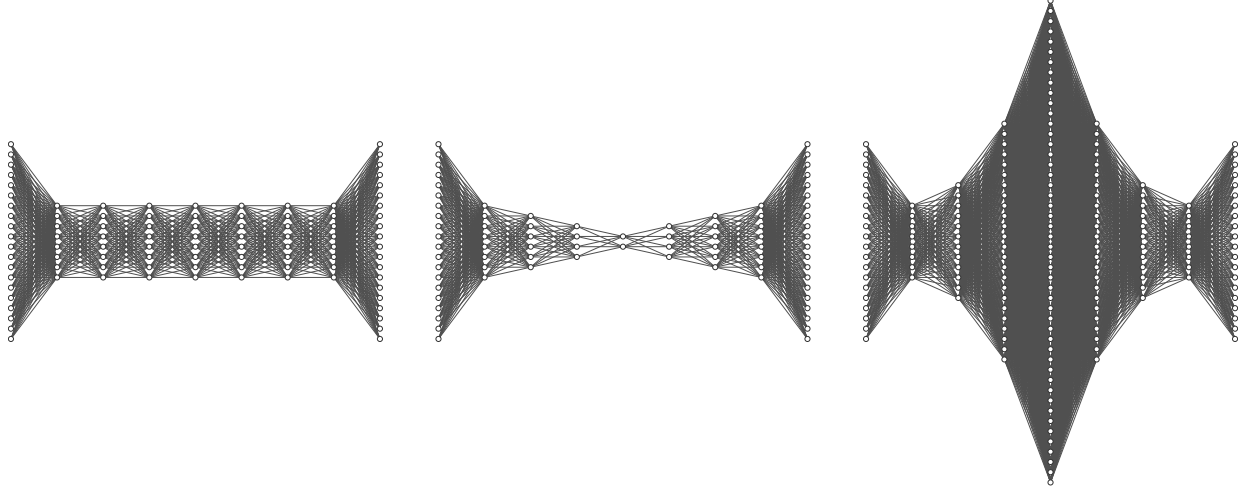


Figure 1: Neural network structures tested: uniform (*left*), converging-diverging (*middle*), and diverging-converging (*right*).

is we directly approximate  $\mathbf{f}_r$ , a mapping between low-dimensional input and output spaces, using nonlinear basis functions. We will show in our numerical experiments (Section 4) that this approximation, when sufficiently trained, mitigates some parametric robustness and stability issues of traditional hyperreduction techniques, such as (D)EIM, that approximate the mapping  $(\boldsymbol{\tau}, t, \boldsymbol{\mu}) \mapsto \mathbf{f}(\bar{\mathbf{u}} + \Phi\boldsymbol{\tau}, t, \boldsymbol{\mu})$  (low-dimensional input space, high-dimensional output space) using a linear basis.

The computational complexity of a single pass through a FCNN with  $M + 2$  layers with the  $i$ th layer consisting of  $m_i$  neurons,  $i = 0, \dots, M + 1$ , where layer 0 is the input and layer  $M + 1$  is the output, is  $\mathcal{O}(\sum_{i=1}^{M+1} m_{i-1}m_i)$ , which can be seen from a simple analogy to dense matrix-vector multiplication. In our case,  $m_0 = k_{\mathbf{u}} + N_{\boldsymbol{\mu}} + 1$  and  $m_{M+1} = k_{\mathbf{u}}$ . Therefore evaluation of the approximate velocity function  $(\boldsymbol{\tau}, t, \boldsymbol{\mu}, \boldsymbol{\nu}) \mapsto \hat{f}_r(\boldsymbol{\tau}, t, \boldsymbol{\mu}, \boldsymbol{\nu})$  scales quadratically with the breadth of the network and linearly in the depth:  $\mathcal{O}(k_{\mathbf{u}}m_1 + N_{\boldsymbol{\mu}}m_1 + k_{\mathbf{u}}m_M + \sum_{i=2}^M m_{i-1}m_i)$ . In the special case where all hidden layers are the same size  $m_i = m$  for  $i = 1, \dots, M$ , this reduces to  $\mathcal{O}(k_{\mathbf{u}}m + N_{\boldsymbol{\mu}}m + Mm^2)$ . The cost to evaluate the Jacobian  $(\boldsymbol{\tau}, t, \boldsymbol{\mu}, \boldsymbol{\nu}) \mapsto \frac{\partial \hat{f}_r}{\partial \boldsymbol{\tau}}(\boldsymbol{\tau}, t, \boldsymbol{\mu}, \boldsymbol{\nu})$  using automatic differentiation is within a constant factor of the cost for the velocity function itself [63, 64]. Therefore the cost of an entire implicit time step is  $\mathcal{O}(k_{\mathbf{u}}^3 + k_{\mathbf{u}}m_1 + N_{\boldsymbol{\mu}}m_1 + k_{\mathbf{u}}m_M + \sum_{i=2}^M m_{i-1}m_i)$  assuming a direct solver is used for the linear system. In the special case where all hidden layers are the same size, this reduces to  $\mathcal{O}(k_{\mathbf{u}}^3 + k_{\mathbf{u}}m + N_{\boldsymbol{\mu}}m + Mm^2)$ . Assuming the breadth ( $m$ ) and depth ( $M$ ) of the network scale independently of  $N_{\mathbf{u}}$ , we expect this approach to be efficient because the dependence on the large dimension has been removed. If we require the network breadth and depth to be on the order of the size of the reduced basis, i.e.,  $m \sim \mathcal{O}(k_{\mathbf{u}})$  and  $M \sim \mathcal{O}(k_{\mathbf{u}})$ , the complexity of a time step reduces to  $\mathcal{O}(k_{\mathbf{u}}^3 + N_{\boldsymbol{\mu}}k_{\mathbf{u}})$ . This shows the bottleneck caused by the nonlinear terms has been completely eliminated using the proposed FCNN approximation of the nonlinear velocity function with  $\mathcal{O}(k_{\mathbf{u}})$  layers and neurons per layer because, asymptotically, the cost is similar to that of a direct solve with the reduced Jacobian matrix. A similar result follows with broader, shallower networks, e.g.,  $m \sim \mathcal{O}(k_{\mathbf{u}}^{3/2})$  and  $M \sim \mathcal{O}(1)$ , with complexity per time step:  $\mathcal{O}(k_{\mathbf{u}}^3 + N_{\boldsymbol{\mu}}k_{\mathbf{u}}^{3/2})$ . Similarly, deeper, narrower networks can be used, e.g.,  $m \sim \mathcal{O}(k_{\mathbf{u}}^{1/2})$  and  $M \sim \mathcal{O}(k_{\mathbf{u}}^2)$ , with a complexity per time step of  $\mathcal{O}(k_{\mathbf{u}}^3 + N_{\boldsymbol{\mu}}k_{\mathbf{u}}^{1/2})$ . The number of parameters ( $N_{\boldsymbol{\mu}}$ ) is usually small and always independent of  $k_{\mathbf{u}}$ , therefore the dominant complexity for all the network structures mentioned is  $\mathcal{O}(k_{\mathbf{u}}^3)$ .

#### 4. Numerical experiments

In this section, we test the accuracy, stability, and parametric robustness of the proposed ROM-NN method using two dynamical systems that result from the semi-discretization of nonlinear, hyperbolic PDEs. We compare the performance of the ROM-NN method to a standard Galerkin-POD ROM, which provides a theoretical lower bound on the accuracy of the ROM-NN, and the most popular intrusive hyperreduction

method, (D)EIM. For both problems, we define the parameter space  $\mathcal{D}$  and introduce two subsets  $\Xi_0 \subset \Xi^* \subset \mathcal{D}$ , where  $\Xi_0$  are the parameters used to train the reduced-order models and  $\Xi^*$  are all parameters where the accuracy of the models is tested (includes the training points). Recall the definition of the parametric HDM solution  $\mathbf{u}$  (1) and its approximation provided by the ROM  $\mathbf{u}_r$  (2), (D)EIM  $\mathbf{u}_d$  (9), and ROM-NN  $\mathbf{u}_n$  (13). For a given parameter  $\boldsymbol{\mu} \in \mathcal{D}$ , we quantify the error between the HDM solution  $\mathbf{u}(\cdot, \boldsymbol{\mu})$  and an approximate solution  $\mathbf{v}(\cdot, \boldsymbol{\mu})$  as

$$\epsilon(\mathbf{v}; \boldsymbol{\mu}) := \sqrt{\frac{\sum_{i=1}^{N_t} \|\mathbf{v}(t_i, \boldsymbol{\mu}) - \mathbf{u}(t_i, \boldsymbol{\mu})\|^2}{\sum_{i=1}^{N_t} \|\mathbf{u}(t_i, \boldsymbol{\mu})\|^2}}. \quad (16)$$

Therefore the error in the ROM, (D)EIM, and ROM-NN solutions are

$$\epsilon_r(\boldsymbol{\mu}) := \epsilon(\mathbf{u}_r; \boldsymbol{\mu}), \quad \epsilon_d(\boldsymbol{\mu}) := \epsilon(\mathbf{u}_d; \boldsymbol{\mu}), \quad \epsilon_n(\boldsymbol{\mu}) := \epsilon(\mathbf{u}_n; \boldsymbol{\mu}), \quad (17)$$

respectively. In the rest of this section, we will consider the statistics (minimum, maximum, and median) of these error metrics over the training set  $\Xi_0$  and testing set  $\Xi^* \setminus \Xi_0$ . In this work, we do not compare the computational cost of the HDM, ROM, (D)EIM, and ROM-NN because it is heavily dependent on the implementation and a number algorithmic choices, e.g., choice of linear solver.

#### 4.1. One-dimensional viscous Burgers' equation

The first numerical experiment we consider is solution of the one-dimensional, parametrized, viscous Burgers' equation in the domain  $\Omega := (0, 1)$ , where  $u : \Omega \times [0, T] \times \mathcal{D} \rightarrow \mathbb{R}$  solves

$$\begin{aligned} \partial_t u(x, t, \boldsymbol{\mu}) + u(x, t, \boldsymbol{\mu}) \partial_x u(x, t, \boldsymbol{\mu}) &= \nu(\boldsymbol{\mu}) \partial_{xx} u(x, t, \boldsymbol{\mu}) + g(x, \boldsymbol{\mu}), & x \in (0, 1), \quad t \in [0, T], \quad \boldsymbol{\mu} \in \mathcal{D}, \\ u(0, t, \boldsymbol{\mu}) &= 0, \quad u(1, t, \boldsymbol{\mu}) = 0, & t \in [0, T], \quad \boldsymbol{\mu} \in \mathcal{D}. \end{aligned} \quad (18)$$

The time interval is taken as  $T = 1$  and the parameter space is  $\mathcal{D} := [0.01, 0.1] \times [2, 3] \times [0, 1] \subset \mathbb{R}^3$ . For any  $\boldsymbol{\mu} \in \mathcal{D}$  where  $\boldsymbol{\mu} = (\mu_1, \mu_2, \mu_3)$ , the parametrized viscosity and source term are defined as

$$\nu(\boldsymbol{\mu}) = \mu_1, \quad g(x, \boldsymbol{\mu}) = \mu_2 e^{\mu_3 x}. \quad (19)$$

The PDE is discretized in space using 200 linear finite elements with essential boundary conditions strongly enforced to yield a dynamical system of the form (1) with a total of  $N_{\mathbf{u}} = 199$  spatial degrees of freedom. The dynamical system is discretized in time using the two-stage diagonally implicit Runge-Kutta method [65] with 100 time steps.

For this problem, we define the testing set  $\Xi^*$  as the uniform sampling of  $\mathcal{D}$  on a  $5 \times 5 \times 5$  grid for a total of  $|\Xi^*| = 125$  parameter configurations. We consider two training sets:  $\Xi_0^a, \Xi_0^b$  are the uniform samplings of  $\mathcal{D}$  on a  $2 \times 2 \times 2$  and  $3 \times 3 \times 3$  grid, respectively. By construction,  $\Xi_0^a \subset \Xi_0^b \subset \Xi^*$ . For both training sets, we construct a POD-Galerkin ROM without hyperreduction, accelerated with (D)EIM, and accelerated with the neural network approximation of  $\mathbf{f}_r$  using  $k_{\mathbf{u}} = 8$  and test each model on all points in  $\Xi^*$ .

The reduced-order model without hyperreduction is the most stable and accurate method, which is expected since it computes the velocity function  $\mathbf{f}_r$  exactly. Nonlinear approximation via (D)EIM is the least accurate approach and even goes unstable for a number of training and testing points for this small basis size. The neural network approach to approximate the nonlinear terms is more accurate than (D)EIM and is stable for all points in  $\Xi^*$ . These observations are taken from Figures 2 and 3, which contain the PDE state vector computed with each model at several instances in time for various points in  $\Xi^*$  and Figure 4 that directly compares the accuracy of (D)EIM and ROM-NN.

For the training set  $\Xi_0^a$ , the minimum error across both the training and testing sets are comparable for (D)EIM and ROM-NN. Since (D)EIM is unstable on both training and testing points, the maximum error is large. The ROM-NN approach is stable for all points in  $\Xi^*$ ; however, its maximum error on the test set  $\Xi^* \setminus \Xi_0^a$  is large ( $\approx 22\%$ ). The median error for the ROM-NN less than 3% on the training set and 5% on the testing set, while (D)EIM has median errors up to five times larger (16% training, 11% testing) (Table 1). By increasing the training set to  $\Xi_0^b$  and keeping the ROM size fixed ( $k_{\mathbf{u}} = 8$ ), the stability of (D)EIM further degrades (15 unstable points in  $\Xi^*$ ), but the accuracy improves for stable configurations (median

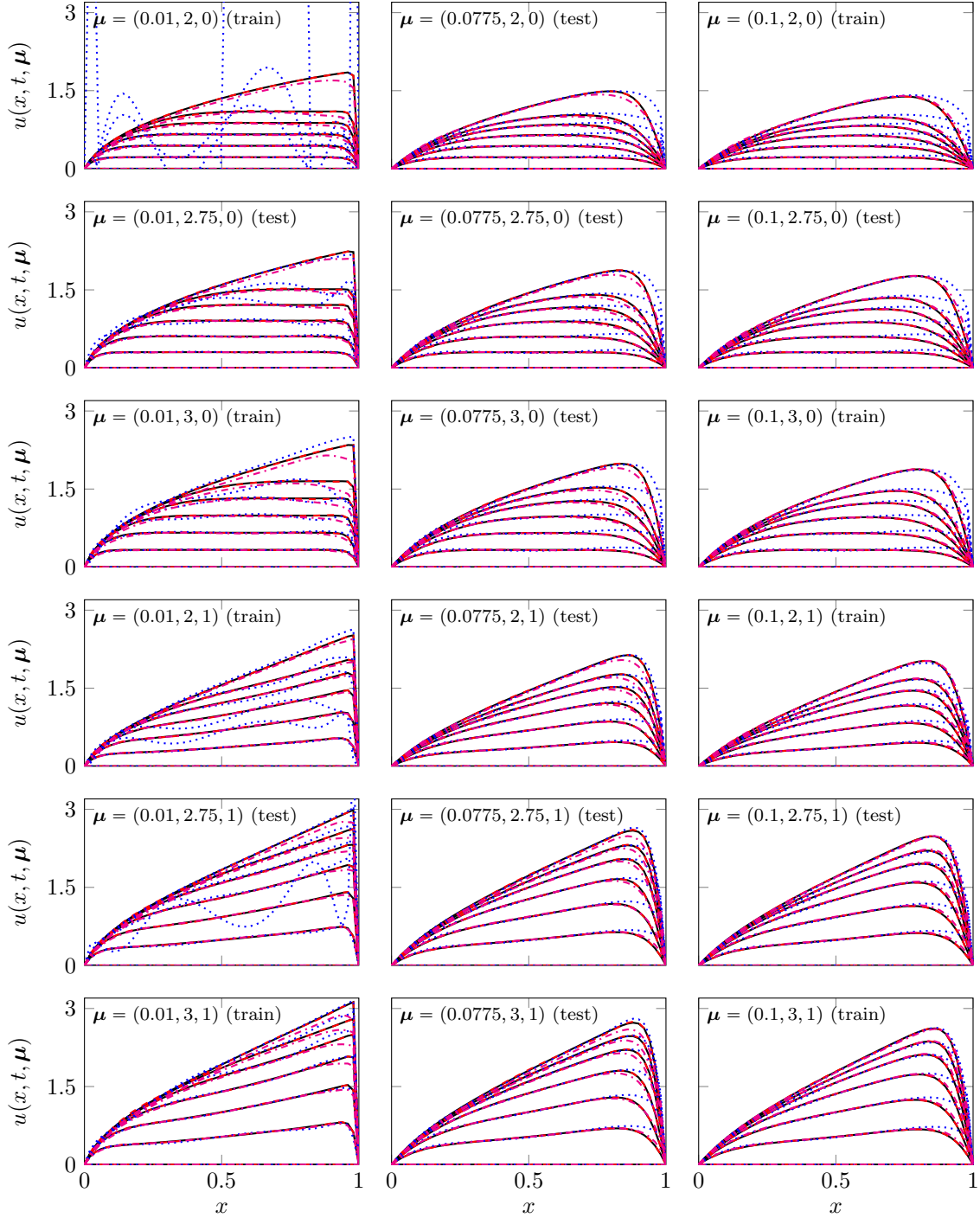


Figure 2: Snapshots of viscous Burgers' equation ( $t = 0, 0.11, 0.22, 0.33, 0.44, 0.55, 1$ ) at various parameter configurations using HDM (—), ROM (---), (D)EIM (·····), ROM-NN (-·-·-). The model reduction methods are trained using 8 parameter samples ( $\Xi_0^g$ ) for a total of 800 snapshots and compressed to a size  $k_u = 8$ . In most cases, including both training and testing configuration, the ROM-NN model is more accurate than the (D)EIM model and does not exhibit the same stability issues.

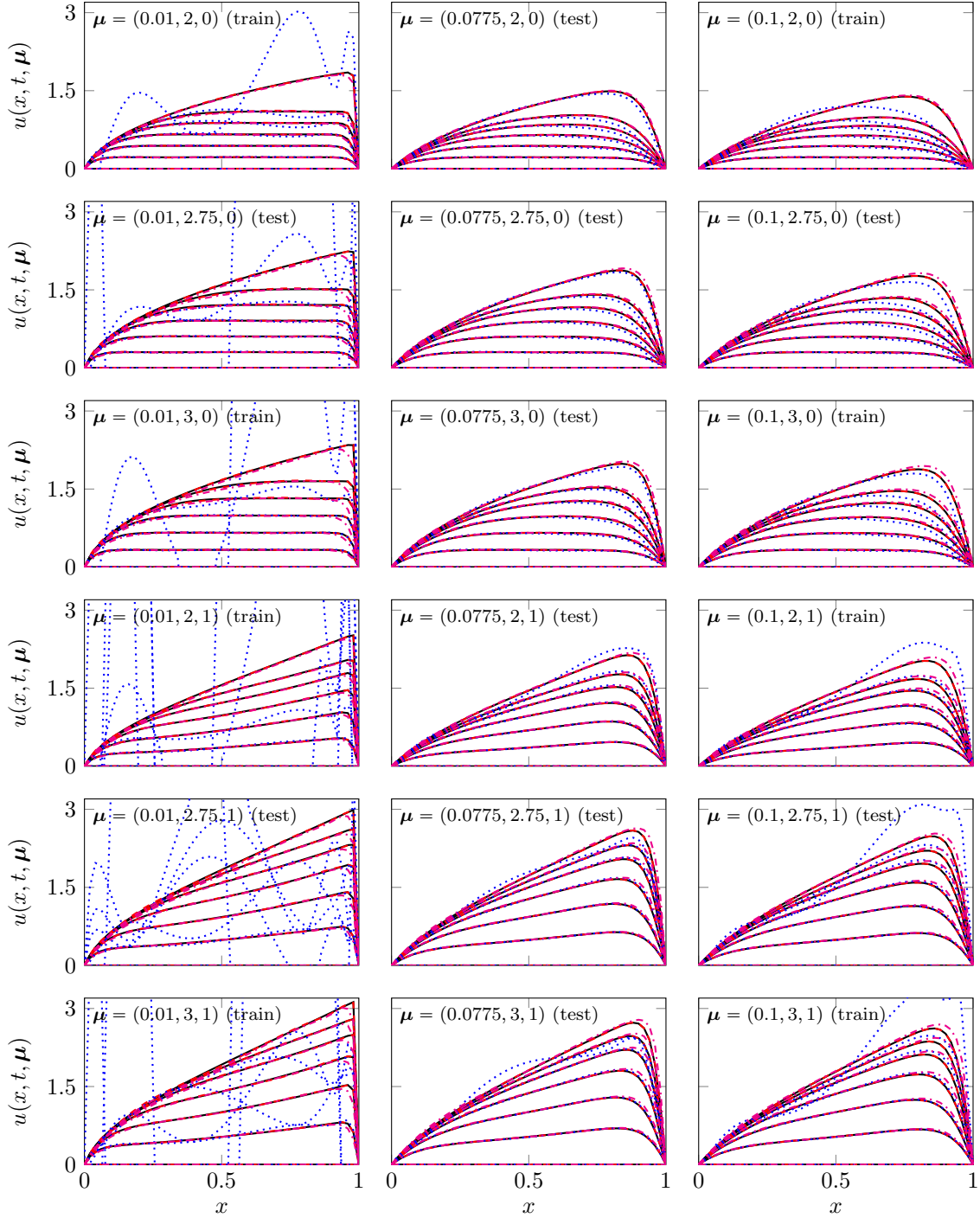


Figure 3: Snapshots of viscous Burgers' equation ( $t = 0, 0.11, 0.22, 0.33, 0.44, 0.55, 1$ ) at various parameter configurations using HDM (—), ROM (---), (D)EIM (·····), ROM-NN (-·-·-). The model reduction methods are trained using 27 parameter samples ( $\Xi_0^p$ ) for a total of 2700 snapshots and compressed to a size  $k_u = 8$ . In most cases, including both training and testing configuration, the ROM-NN model is more accurate than the (D)EIM model and does not exhibit the same stability issues.

Table 1: Summary of the performance of the model reduction methods trained on  $\Xi_0^a$ , compressed to  $k_u = 8$ , and tested on  $\Xi^*$ . The error statistics are reported for the training set  $\Xi_0^a$  and testing set  $\Xi^* \setminus \Xi_0^a$  separately. The ROM-NN is stable for all training and testing points considered and has a median error less than 3% on the training set and about 5% on the testing set. The (D)EIM method goes unstable at a number of training and testing point and has a median error greater than 10%.

	ROM		(D)EIM		ROM-NN	
	Train set	Test set	Train set	Test set	Train set	Test set
Unstable (#)	0	0	1	5	0	0
Minimum error	2.58e-03	1.48e-03	2.81e-02	3.07e-02	1.68e-02	2.28e-02
Maximum error	7.05e-03	2.54e-02	1.99e+01	5.49e+02	6.17e-02	2.25e-01
Median error	4.66e-03	5.84e-03	1.58e-01	1.12e-01	2.71e-02	5.24e-02

Table 2: Summary of the performance of the model reduction methods trained on  $\Xi_0^b$ , compressed to  $k_u = 8$ , and tested on  $\Xi^*$ . The error statistics are reported for the training set  $\Xi_0^b$  and testing set  $\Xi^* \setminus \Xi_0^b$  separately. The ROM-NN is stable for all training and testing points considered and has a median error less than 3% on both the training and testing set. The (D)EIM method goes unstable at a number of training and testing point and has a median error greater than 10%.

	ROM		(D)EIM		ROM-NN	
	Train set	Test set	Train set	Test set	Train set	Test set
Unstable (#)	0	0	6	9	0	0
Minimum error	1.43e-03	1.54e-03	2.95e-02	9.39e-03	8.09e-03	7.58e-03
Maximum error	8.62e-03	1.81e-02	2.96e+02	1.65e+03	6.26e-02	5.99e-02
Median error	2.67e-03	2.51e-03	1.22e-01	1.16e-01	2.78e-02	2.47e-02

errors decrease). The ROM-NN training errors are similar to the case where  $\Xi_0^a$  is used as the training set, but the errors on the testing set become smaller suggesting the additional training leads to better prediction. The median and maximum errors of the ROM-NN for both training and testing sets are roughly 3% and 6%, respectively (Table 2).

#### 4.2. Two-dimensional premixed $H_2$ -air flame model

The second numerical experiment we consider is solution of a simplified model of a premixed  $H_2$ -air flame at a constant and uniform pressure, in a constant, divergence-free velocity field, and with constant, uniform diffusivities for all species and temperature in the domain  $\Omega := [0, L_x] \times [0, L_y]$ , where  $L_x = 18\text{mm}$  and  $L_y = 9\text{mm}$ , over the time interval  $[0, T]$ ,  $T = 0.06\text{s}$ . The one-step reaction mechanism is  $2H_2 + O_2 \rightarrow 2H_2O$ . The PDE model of this system [66] is

$$\begin{aligned}
 \partial_t U(x, t, \boldsymbol{\mu}) - \kappa \Delta U(x, t, \boldsymbol{\mu}) + \beta \cdot \nabla U(x, t, \boldsymbol{\mu}) &= \mathcal{N}(U, \boldsymbol{\mu}), & x \in \Omega, & \quad t \in [0, T], & \quad \boldsymbol{\mu} \in \mathcal{D}, \\
 U(x, t, \boldsymbol{\mu}) &= U_D(x), & x \in \Gamma_D, & \quad t \in [0, T], & \quad \boldsymbol{\mu} \in \mathcal{D}, \\
 \nabla U(x, t, \boldsymbol{\mu}) \cdot \boldsymbol{n}(x) &= 0, & x \in \Gamma_N, & \quad t \in [0, T], & \quad \boldsymbol{\mu} \in \mathcal{D}, \\
 U(x, 0, \boldsymbol{\mu}) &= U_0, & x \in \Omega, & & \quad \boldsymbol{\mu} \in \mathcal{D}
 \end{aligned} \tag{20}$$

with solution

$$U : \Omega \times [0, T] \times \mathcal{D} \rightarrow \mathbb{R}^4, \quad (x, t, \boldsymbol{\mu}) \mapsto \begin{bmatrix} Y_F(x, t, \boldsymbol{\mu}) \\ Y_O(x, t, \boldsymbol{\mu}) \\ Y_P(x, t, \boldsymbol{\mu}) \\ \Theta(x, t, \boldsymbol{\mu}) \end{bmatrix}, \tag{21}$$

where  $\boldsymbol{n} : \partial\Omega \rightarrow \mathbb{R}^2$  is the outward unit normal,  $Y_i : \Omega \times [0, T] \times \mathcal{D} \rightarrow \mathbb{R}$  is the mass fraction of the hydrogen fuel ( $i = F$ ), oxygen ( $i = O$ ), and water product ( $i = P$ ), and  $\Theta : \Omega \times [0, T] \times \mathcal{D} \rightarrow \mathbb{R}$  is the temperature. The domain boundary is split into six segments (Figure 5)

$$\partial\Omega = \bigcup_{i=1}^6 \Gamma_i, \quad \Gamma_D := \bigcup_{i=1}^3 \Gamma_i, \quad \Gamma_N := \bigcup_{i=4}^6 \Gamma_i \tag{22}$$

with the following essential boundary conditions prescribed on  $\Gamma_D \subset \partial\Omega$

$$U_D : \Omega \rightarrow \mathbb{R}^4, \quad x \mapsto \begin{cases} (0, 0, 0, 300) & x \in \Gamma_1 \cup \Gamma_3 \\ (0.0282, 0.2259, 0, 950) & x \in \Gamma_2 \end{cases} \tag{23}$$

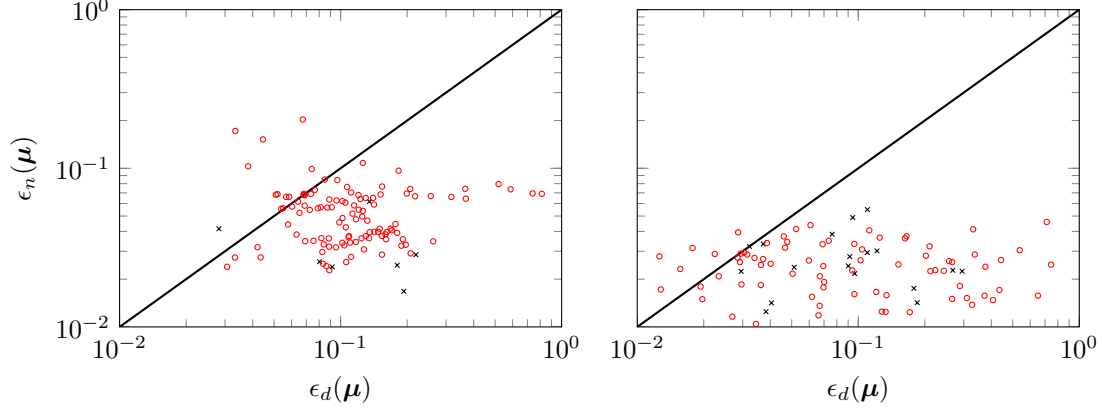


Figure 4: Comparison of the error in the (D)EIM and ROM-NN ( $k_u = 8$ ) with respect to the HDM solution when trained with  $\Xi_0^a$  (left) or  $\Xi_0^b$  (right) for each point in  $\Xi^*$ . The individual marks correspond to the (D)EIM error vs. the ROM error for training ( $\times$ ) and testing ( $\circ$ ) points. All entries that lie below the line of identity (—) correspond to parameters where the ROM-NN is more accurate than (D)EIM. For both training cases, far more points lie below the line of identity indicating the ROM-NN is more accurate across the testing set  $\Xi^*$  than (D)EIM.

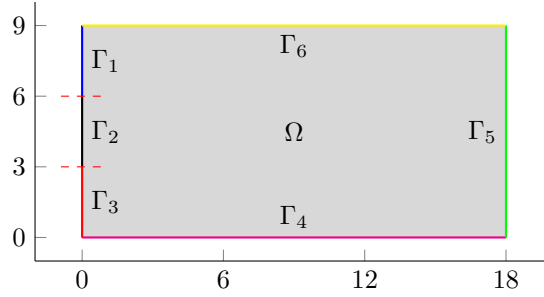


Figure 5: Schematic setup for the hydrogen-air flame (units: mm).

and homogeneous natural boundary conditions on  $\Gamma_N \subset \partial\Omega$ . The nonlinear reaction source term is of Arrhenius type and modeled as in Cuenot and Poinot [67] as  $\mathcal{N}(U, \boldsymbol{\mu}) = [\mathcal{N}_F(U, \boldsymbol{\mu}), \mathcal{N}_O(U, \boldsymbol{\mu}), \mathcal{N}_P(U, \boldsymbol{\mu}), \mathcal{N}_\Theta(U, \boldsymbol{\mu})]$ , where

$$\begin{aligned} \mathcal{N}_i(U, \boldsymbol{\mu}) &= -\nu_i \left( \frac{W_i}{\rho} \right) \left( \frac{\rho Y_F}{W_F} \right)^{\nu_F} \left( \frac{\rho Y_O}{W_O} \right)^{\nu_O} A(\boldsymbol{\mu}) \exp \left( -\frac{E(\boldsymbol{\mu})}{R\Theta} \right) \\ \mathcal{N}_\Theta(U, \boldsymbol{\mu}) &= \mathcal{N}_P(U, \boldsymbol{\mu})Q \end{aligned} \quad (24)$$

for  $i = F, O, P$ . The divergence-free velocity field is  $\beta = (50, 0)$  cm/sec. The diffusivities are  $\kappa = 2.0$  cm<sup>2</sup>/sec and the density of the mixture is  $\rho = 1.39 \times 10^{-3}$  gr/cm<sup>3</sup>. The molecular weights are  $W_F = 2.016$ ,  $W_O = 31.9$ ,  $W_P = 18$  gr/mol, the stoichiometric coefficients are  $\nu_F = 2$ ,  $\nu_O = 1$ ,  $\nu_P = 2$ , the heat of reaction is  $Q = 9800$ K, and the universal gas constant is  $R = 8.314472$  J/(mol K). The parameter space is taken as  $\mathcal{D} := [2.3375 \times 10^{12}, 6.2 \times 10^{12}] \times [5625.5, 9000]$ . For any  $\boldsymbol{\mu} \in \mathcal{D}$  where  $\boldsymbol{\mu} = (\mu_1, \mu_2)$ , the parametrized pre-exponential factor and activation energy are taken as

$$A(\boldsymbol{\mu}) = \mu_1, \quad E(\boldsymbol{\mu}) = \mu_2. \quad (25)$$

At  $t = 0$ , the domain is considered empty at a temperature of 300K, i.e.,  $U_0 = (0, 0, 0, 300)$ . The PDE is discretized in space using the finite difference method on a grid of  $40 \times 20$  with essential boundary conditions strongly enforced to yield a dynamical system of the form (1) with a total of  $N_u = 2736$  spatial degrees of freedom. The dynamical system is discretized in time using a two-stage diagonally implicit Runge-Kutta method with 50 time steps; see Figure 6 for solution snapshots for a representative parameter configuration.

For this problem, we define the testing set  $\Xi^*$  as the uniform sampling of  $\mathcal{D}$  on a  $7 \times 7$  grid for a total of  $|\Xi^*| = 49$  test points. The training set is a uniform sampling of  $\mathcal{D}$  on a  $4 \times 4$  grid, respectively. By construction,  $\Xi_0 \subset \Xi^*$ . Similar to the previous section, we construct a POD-Galerkin ROM without

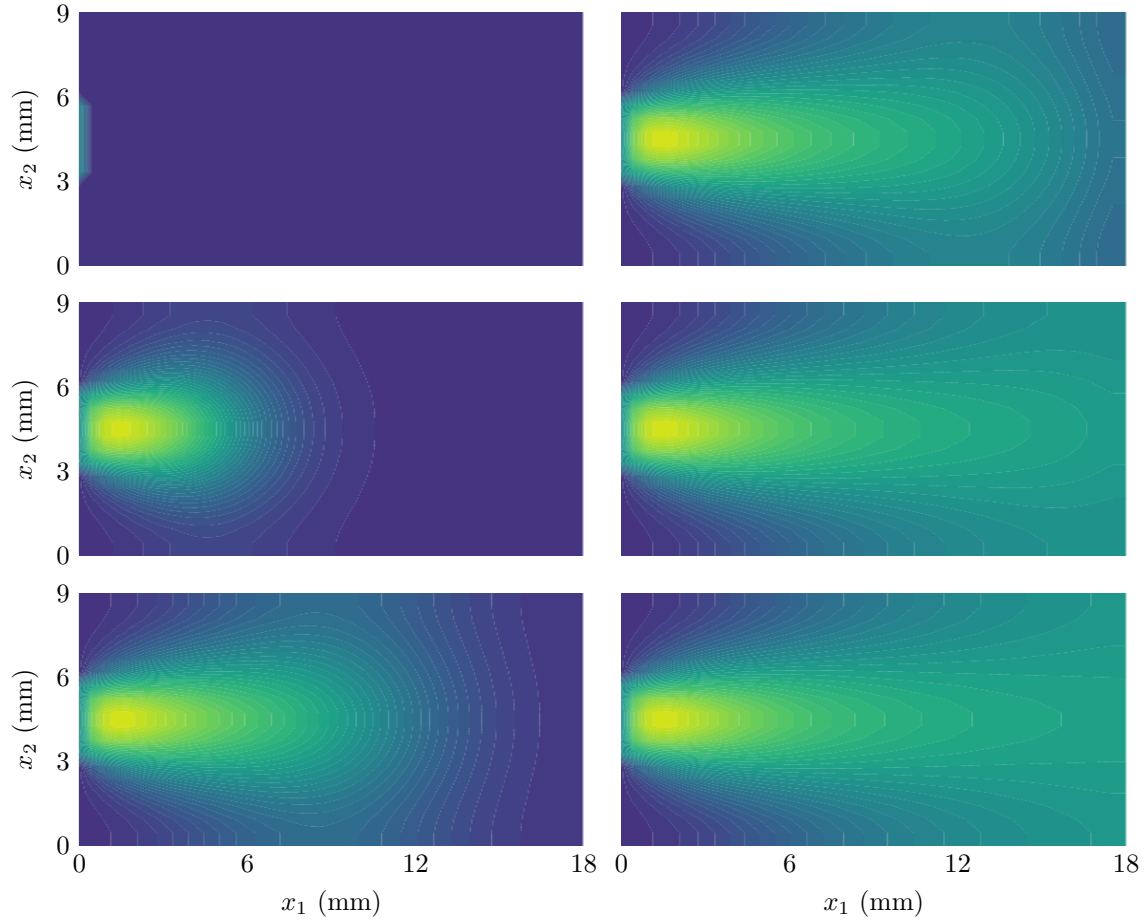


Figure 6: Snapshots of advection-diffusion-reaction temperature ( $\Theta(x, t, \boldsymbol{\mu})$ ) field ( $t = 0, 0.012, 0.024, 0.036, 0.048, 0.06$ ; top-to-bottom then left-to-right) at  $\boldsymbol{\mu} = (5.1125 \times 10^{12}, 6187.91667)$  computed using the HDM.

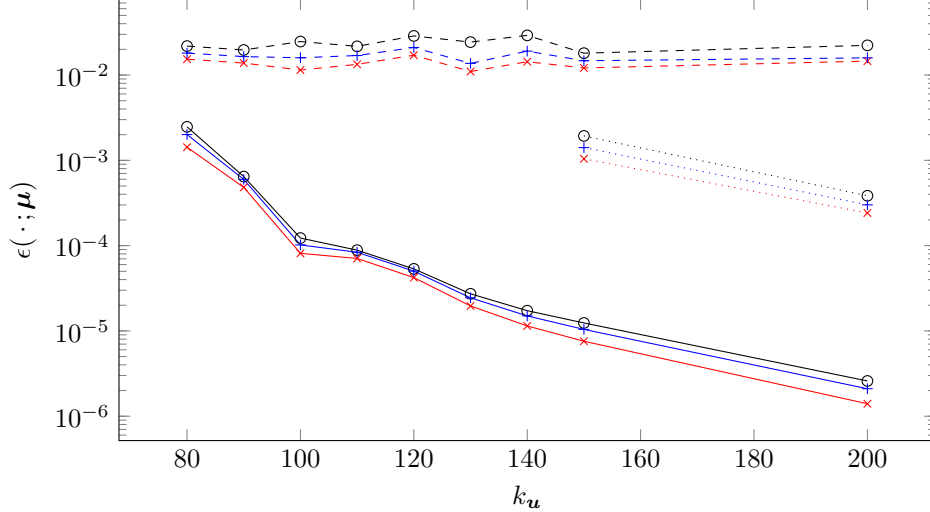


Figure 7: The maximum (circle), minimum (cross), and median (plus) error of the ROM (solid), (D)EIM (dotted), and ROM-NN (dashed) over the set  $\Xi^*$ . While the ROM error statistics demonstrate deep convergence under refinement of  $k_u$ , the ROM-NN does not (expected because  $\hat{f}$  has more inputs/outputs as  $k_u$  increases and therefore becomes more difficult to train). Even though the ROM-NN does not have deep convergence, its maximum and median errors are small (3%). (D)EIM is unstable for  $k_u < 150$ ; however, once the basis is sufficiently large  $k_u \geq 150$  for stability, it is more accurate than the ROM-NN. Legend: maximum ROM error ( $\text{---}\circ\text{---}$ ), minimum ROM error ( $\text{---}\times\text{---}$ ), median ROM error ( $\text{---}+\text{---}$ ), maximum (D)EIM error ( $\cdots\circ\cdots$ ), minimum (D)EIM error ( $\cdots\times\cdots$ ), median (D)EIM error ( $\cdots+\cdots$ ), maximum ROM-NN error ( $\text{---}\ominus\text{---}$ ), minimum ROM-NN error ( $\text{---}\times\text{---}$ ), median ROM-NN error ( $\text{---}+\text{---}$ ).

hyperreduction, one accelerated with (D)EIM, and one accelerated with the neural network for a range of basis sizes ( $k_u$ ) and subsequently test each model on all points in  $\Xi^*$ .

The reduced-order model without hyperreduction is the most stable and accurate method and demonstrates deep convergence under refinement of  $k_u$ , even when error metric is aggregated over both testing and training points. For this problem, (D)EIM was highly unstable; a basis of size  $k_u = 150$  was required for stability, while the other methods were stable for a basis of size  $k_u = 80$ . When (D)EIM is stable, it is more accurate than the proposed ROM-NN method. The ROM-NN method is stable for all basis sizes considered, but does not exhibit deep convergence (the error is about 2% for basis sizes  $k_u \in [80, 200]$ ). We have run extensive numerical tests to confirm this is due to the scaling of the entries of  $\mathbf{f}_r$ , which can vary by up to seven orders of magnitude for this problem. This implies the loss function used to train the FCNN is heavily biased toward the important coefficients and the smallest coefficients are all but ignored in the training. As a result, the relative error of the small coefficients (required for deep convergence) is large. Weighting the loss function to offset the massively different scale of the loss function terms causes the approximation of small coefficients to improve, but the accuracy of the large (important) coefficients degrades for the networks considered in this work, which causes the overall error to increase. Because the ROM-NN does not exhibit deep convergence, there is little point in refining the basis beyond  $k_u = 80$  because the reduction in error is negligible. The maximum and median errors of the ROM-NN solution ( $k_u = 80$ ) across all training and testing parameters are small (2 – 3%) (Figure 7).

## 5. Conclusion

This work developed a *non-intrusive* acceleration technique for projection-based model reduction of nonlinear dynamical systems using deep neural networks. The approach is non-intrusive in the sense that it treats both the original dynamical system and neural network code as black boxes. The method is trained using the same HDM solutions computed to train the reduced basis, i.e., no new simulations are required to train the neural network approximation of the ROM velocity function, only evaluations of the ROM velocity at existing snapshots. Unlike traditional hyperreduction methods, this does not require modification of the underlying dynamical system code because, once the neural network is trained, only forward propagation (and symbolic differentiation) through the network is required to compute the approximate velocity function

and its derivative. Aside from the benefit of non-intrusivity, the proposed method is more stable and accurate at both training and testing points in the limit of a small basis than the popular (D)EIM hyperreduction for the two dynamical systems considered (semi-discretizations of nonlinear, hyperbolic PDEs). Given we used uniform sampling to train the ROM-NN, this approach may be most appropriate for problems with a limited number of parameters. Future work will explore whether the amount of training can be reduced using POD-Greedy sampling [53] without sacrificing stability or parametric robustness. We will also perform a careful study of the computational cost of the proposed approach and the benefits of using GPUs to train and pass through the neural network in future work.

## References

- [1] M. J. Zahr, P.-O. Persson, An adjoint method for a high-order discretization of deforming domain conservation laws for optimization of flow problems, *Journal of Computational Physics* 326 (Supplement C) (2016) 516 – 543. doi:<https://doi.org/10.1016/j.jcp.2016.09.012>.
- [2] M. J. Zahr, P.-O. Persson, J. Wilkening, A fully discrete adjoint method for optimization of flow problems on deforming domains with time-periodicity constraints, *Computers & Fluids* 139 (2016) 130 – 147. doi:[10.1016/j.compfluid.2016.05.021](https://doi.org/10.1016/j.compfluid.2016.05.021).
- [3] J. Wang, M. Zahr, P.-O. Persson, Energetically optimal flapping flight based on a fully discrete adjoint method with explicit treatment of flapping frequency, in: Proc. of the 23rd AIAA Computational Fluid Dynamics Conference, American Institute of Aeronautics and Astronautics, Denver, Colorado, 6/5/2017 – 6/9/2017.
- [4] M. J. Zahr, P.-O. Persson, Energetically optimal flapping wing motions via adjoint-based optimization and high-order discretizations, in: *Frontiers in PDE-Constrained Optimization*, Springer, 2018.
- [5] M. Barrault, Y. Maday, N. Nguyen, A. Patera, An ‘empirical interpolation’ method: application to efficient reduced-basis discretization of partial differential equations, *Comptes Rendus Mathématique* 339 (9) (2004) 667–672.
- [6] S. Chaturantabut, D. Sorensen, Nonlinear model reduction via discrete empirical interpolation, *SIAM Journal on Scientific Computing* 32 (5) (2010) 2737–2764.
- [7] K. Carlberg, D. Amsallem, P. Avery, M. Zahr, C. Farhat, The GNAT nonlinear model reduction method and its application to fluid dynamics problems, in: 6th AIAA Theoretical Fluid Mechanics Conference, 2011, p. 3112.
- [8] C. Farhat, T. Chapman, P. Avery, [Structure-preserving, stability, and accuracy properties of the energy-conserving sampling and weighting method for the hyper reduction of nonlinear finite element dynamic models](https://doi.org/10.1002/nme.4820), *Internat. J. Numer. Methods Engrg.* 102 (5) (2015) 1077–1110. doi:[10.1002/nme.4820](https://doi.org/10.1002/nme.4820). URL <https://doi.org/10.1002/nme.4820>
- [9] M. J. Zahr, P. Avery, C. Farhat, A multilevel projection-based model order reduction framework for nonlinear dynamic multiscale problems in structural and solid mechanics, *International Journal for Numerical Methods in Engineering* 112 (8) (2017) 855–881. doi:[10.1002/nme.5535](https://doi.org/10.1002/nme.5535).
- [10] K. Washabaugh, Faster fidelity for better design: A scalable model order reduction framework for steady aerodynamic design applications, Ph.D. thesis, Stanford University (2016).
- [11] C. Audouze, F. De Vuyst, P. B. Nair, Nonintrusive reduced-order modeling of parametrized time-dependent partial differential equations, *Numerical Methods for Partial Differential Equations* 29 (5) (2013) 1587–1628.
- [12] B. Peherstorfer, K. Willcox, Data-driven operator inference for nonintrusive projection-based model reduction, *Computer Methods in Applied Mechanics and Engineering* 306 (2016) 196–215.
- [13] W. Chen, J. S. Hesthaven, B. Junqiang, Y. Qiu, Z. Yang, Y. Tihao, Greedy nonintrusive reduced order model for fluid dynamics, *AIAA Journal* 56 (12) (2018) 4927–4943.

- [14] S.-T. Yeh, X. Wang, C.-L. Sung, S. Mak, Y.-H. Chang, L. Zhang, C. J. Wu, V. Yang, Common proper orthogonal decomposition-based spatiotemporal emulator for design exploration, *AIAA Journal* 56 (6) (2018) 2429–2442.
- [15] M. Rewienski, J. White, A trajectory piecewise-linear approach to model order reduction and fast simulation of nonlinear circuits and micromachined devices, *IEEE Transactions on computer-aided design of integrated circuits and systems* 22 (2) (2003) 155–170.
- [16] N. Dong, J. Roychowdhury, Piecewise polynomial nonlinear model reduction, in: *Proceedings of the 40th annual Design Automation Conference*, ACM, 2003, pp. 484–489.
- [17] M. Cardoso, L. Durlofsky, Linearized reduced-order models for subsurface flow simulation, *Journal of Computational Physics* 229 (3) (2010) 681–700.
- [18] J. He, J. Sætrom, L. Durlofsky, Enhanced linearized reduced-order models for subsurface flow simulation, *Journal of Computational Physics* 230 (23) (2011) 8313–8341.
- [19] S. Trehan, L. Durlofsky, Trajectory piecewise quadratic reduced-order model for subsurface flow, with application to PDE-constrained optimization, *Journal of Computational Physics* 326 (2016) 446–473.
- [20] D. Vasilyev, M. Rewienski, J. White, Macromodel generation for biomems components using a stabilized balanced truncation plus trajectory piecewise-linear approach, *IEEE Transactions on Computer-Aided Design of Integrated Circuits and Systems* 25 (2) (2006) 285–293.
- [21] M. J. Zahr, K. Carlberg, D. Amsallem, C. Farhat, Comparison of model reduction techniques on high-fidelity linear and nonlinear electrical, mechanical, and biological systems, *Tech. rep.*, University of California, Berkeley (2010).
- [22] S. Lee, N. Baker, Basic research needs for scientific machine learning: Core technologies for artificial intelligence, *Tech. rep.*, USDOE Office of Science (SC)(United States) (2018).
- [23] S. Brunton, B. Noack, P. Koumoutsakos, Machine learning for fluid mechanics, *arXiv preprint arXiv:1905.11075*.
- [24] J.-X. Wang, J.-L. Wu, H. Xiao, Physics-informed machine learning approach for reconstructing Reynolds stress modeling discrepancies based on DNS data, *Physical Review Fluids* 2 (3) (2017) 034603.
- [25] P. E. Shanahan, D. Trewartha, W. Detmold, Machine learning action parameters in lattice quantum chromodynamics, *Physical Review D* 97 (9) (2018) 094506.
- [26] S. L. Brunton, J. N. Kutz, *Data-driven Science and Engineering: Machine Learning, Dynamical Systems, and Control*, Cambridge University Press, 2019.
- [27] S. Trehan, K. T. Carlberg, L. J. Durlofsky, Error modeling for surrogates of dynamical systems using machine learning, *International Journal for Numerical Methods in Engineering* 112 (12) (2017) 1801–1827.
- [28] O. San, R. Maulik, Machine learning closures for model order reduction of thermal fluids, *Applied Mathematical Modelling* 60 (2018) 681–710.
- [29] O. San, R. Maulik, Neural network closures for nonlinear model order reduction, *Advances in Computational Mathematics* 44 (6) (2018) 1717–1750.
- [30] S. Pan, K. Duraisamy, Data-driven discovery of closure models, *SIAM Journal on Applied Dynamical Systems* 17 (4) (2018) 2381–2413.
- [31] Z. Y. Wan, P. Vlachas, P. Koumoutsakos, T. Sapsis, Data-assisted reduced-order modeling of extreme events in complex dynamical systems, *PloS one* 13 (5) (2018) e0197704.

- [32] M. Mohebujjaman, L. G. Rebholz, T. Iliescu, Physically constrained data-driven correction for reduced-order modeling of fluid flows, *International Journal for Numerical Methods in Fluids* 89 (3) (2019) 103–122.
- [33] R. Maulik, A. Mohan, B. Lusch, S. Madireddy, P. Balaprakash, Time-series learning of latent-space dynamics for reduced-order model closure, arXiv preprint arXiv:1906.07815.
- [34] C. Mou, H. Liu, D. R. Wells, T. Iliescu, Data-driven correction reduced order models for the quasi-geostrophic equations: A numerical investigation, arXiv preprint arXiv:1908.05297.
- [35] D. Xiao, F. Fang, A. Buchan, C. Pain, I. Navon, A. Muggeridge, Non-intrusive reduced order modelling of the navier–stokes equations, *Computer Methods in Applied Mechanics and Engineering* 293 (2015) 522–541.
- [36] J. N. Kani, A. H. Elsheikh, Dr-rnn: A deep residual recurrent neural network for model reduction, arXiv preprint arXiv:1709.00939.
- [37] A. T. Mohan, D. V. Gaitonde, A deep learning based approach to reduced order modeling for turbulent flow control using lstm neural networks, arXiv preprint arXiv:1804.09269.
- [38] J. S. Hesthaven, S. Ubbiali, Non-intrusive reduced order modeling of nonlinear problems using neural networks, *Journal of Computational Physics* 363 (2018) 55–78.
- [39] Z. Wang, D. Xiao, F. Fang, R. Govindan, C. C. Pain, Y. Guo, Model identification of reduced order fluid dynamics systems using deep learning, *International Journal for Numerical Methods in Fluids* 86 (4) (2018) 255–268.
- [40] O. San, R. Maulik, M. Ahmed, An artificial neural network framework for reduced order modeling of transient flows, *Communications in Nonlinear Science and Numerical Simulation* 77 (2019) 271–287.
- [41] F. Regazzoni, L. Dedè, A. Quarteroni, Machine learning for fast and reliable solution of time-dependent differential equations, *Journal of Computational Physics* 397 (2019) 108852.
- [42] Q. Wang, J. S. Hesthaven, D. Ray, Non-intrusive reduced order modeling of unsteady flows using artificial neural networks with application to a combustion problem, *Journal of computational physics* 384 (2019) 289–307.
- [43] K. Li, J. Kou, W. Zhang, Deep neural network for unsteady aerodynamic and aeroelastic modeling across multiple mach numbers, *Nonlinear Dynamics* 96 (3) (2019) 2157–2177.
- [44] H. F. Lui, W. R. Wolf, Construction of reduced-order models for fluid flows using deep feedforward neural networks, *Journal of Fluid Mechanics* 872 (2019) 963–994.
- [45] X. Xie, G. Zhang, C. G. Webster, Non-intrusive inference reduced order model for fluids using deep multistep neural network.
- [46] S. Pawar, S. Rahman, H. Vaddirreddy, O. San, A. Rasheed, P. Vedula, A deep learning enabler for nonintrusive reduced order modeling of fluid flows, *Physics of Fluids* 31 (8) (2019) 085101.
- [47] Z. L. Jin, Y. Liu, L. J. Durlofsky, Deep-learning-based reduced-order modeling for subsurface flow simulation, arXiv preprint arXiv:1906.03729.
- [48] N. D. Santo, S. Deparis, L. Pegolotti, Data driven approximation of parametrized pdes by reduced basis and neural networks, arXiv preprint arXiv:1904.01514.
- [49] R. Maulik, V. Rao, S. Madireddy, B. Lusch, P. Balaprakash, Using recurrent neural networks for nonlinear component computation in advection-dominated reduced-order models, arXiv:1909.09144.
- [50] D. Amsallem, M. Zahr, C. Farhat, Nonlinear model order reduction based on local reduced-order bases, *Internat. J. Numer. Methods Engrg.* 92 (10) (2012) 891–916.

- [51] L. Sirovich, Turbulence and the dynamics of coherent structures. I. Coherent structures, *Quarterly of Applied Mathematics* 45 (3) (1987) 561–571.
- [52] G. Rozza, D. Huynh, A. Patera, Reduced basis approximation and a posteriori error estimation for affinely parametrized elliptic coercive partial differential equations, *Archives of Computational Methods in Engineering* 15 (3) (2008) 229–275.
- [53] B. Haasdonk, Convergence rates of the POD–Greedy method, *ESAIM: Mathematical Modelling and Numerical Analysis* 47 (3) (2013) 859–873.
- [54] D. Ryckelynck, A priori hyperreduction method: an adaptive approach, *Journal of Computational Physics* 202 (1) (2005) 346–366.
- [55] S. An, T. Kim, D. James, Optimizing cubature for efficient integration of subspace deformations, in: *ACM Transactions on Graphics (TOG)*, Vol. 27, ACM, 2008, p. 165.
- [56] P. Astrid, S. Weiland, K. Willcox, T. Backx, Missing point estimation in models described by proper orthogonal decomposition, *IEEE Transactions on Automatic Control* 53 (10) (2008) 2237–2251.
- [57] P. Tiso, D. Rixen, Discrete empirical interpolation method for finite element structural dynamics, in: *Topics in Nonlinear Dynamics*, Volume 1, Springer, 2013, pp. 203–212.
- [58] M. Yano, Discontinuous Galerkin reduced basis empirical quadrature procedure for model reduction of parametrized nonlinear conservation laws, *Advances in Computational Mathematics* (2019) 1–34.
- [59] K. Carlberg, C. Farhat, J. Cortial, D. Amsallem, [The GNAT method for nonlinear model reduction: Effective implementation and application to computational fluid dynamics and turbulent flows](#), *J. Comput. Phys.* 242 (2013) 623 – 647. doi:<https://doi.org/10.1016/j.jcp.2013.02.028>. URL <http://www.sciencedirect.com/science/article/pii/S0021999113001472>
- [60] D. P. Kingma, J. Ba, Adam: A method for stochastic optimization, arXiv preprint arXiv:1412.6980.
- [61] N. Srivastava, G. Hinton, A. Krizhevsky, I. Sutskever, R. Salakhutdinov, Dropout: a simple way to prevent neural networks from overfitting, *The Journal of Machine Learning Research* 15 (1) (2014) 1929–1958.
- [62] Y. Yao, L. Rosasco, A. Caponnetto, On early stopping in gradient descent learning, *Constructive Approximation* 26 (2) (2007) 289–315.
- [63] W. Baur, V. Strassen, The complexity of partial derivatives, *Theoretical Computer Science* 22 (3) (1983) 317–330.
- [64] A. Griewank, A. Walther, *Evaluating Derivatives: Principles and Techniques of Algorithmic Differentiation*, Vol. 105, SIAM, 2008.
- [65] R. Alexander, Diagonally implicit Runge–Kutta methods for stiff ODE’s, *SIAM Journal on Numerical Analysis* 14 (6) (1977) 1006–1021.
- [66] M. Buffoni, K. Willcox, Projection-based model reduction for reacting flows, in: *40th Fluid Dynamics Conference and Exhibit*, 2010, p. 5008.
- [67] B. Cuenot, T. Poinso, Asymptotic and numerical study of diffusion flames with variable Lewis number and finite rate chemistry, *Combustion and Flame* 104 (1-2) (1996) 111–137.